Monolithic multichannel ultraviolet detector arrays and continuous phase evolution in $Mg_xZn_{1-x}O$ composition spreads

I. Takeuchi,[a] W. Yang, K.-S. Chang,[b] M. A. Aronova, and T. Venkatesan
Center for Superconductivity Research, Department of Physics, University of Maryland, College Park, Maryland 20742

R. D. Vispute[c]
Blue Wave Semiconductors, Columbia, Maryland 21045

L. A. Bendersky
National Institute of Standards and Technology, Gaithersburg, Maryland 20899

(Received 22 July 2003; accepted 16 September 2003; publisher error corrected 25 February 2004)

We have fabricated $Mg_xZn_{1-x}O$ epitaxial composition spreads where the composition across the chip is linearly varied from ZnO to MgO. By using a scanning x-ray microdiffractometer and transmission electron microscopy, we have mapped the phase evolution across the spread. We have discovered a unique growth relationship between cubic and hexagonal $Mg_xZn_{1-x}O$ where their basal planes are coincident in the phase-separated region of the phase diagram where $0.37 \leqslant x \leqslant 0.6$. The continuously changing band gap across the spread is used as a basis for compact broadband photodetector arrays with a range of detection wavelengths separately active at different locations on the spread film. The composition-spread photodetector is demonstrated in the wavelength range of 290–380 nm using the ZnO to $Mg_{0.4}Zn_{0.6}O$ region of the spread. © *2003 American Institute of Physics.* [DOI: 10.1063/1.1623923]

I. INTRODUCTION

ZnO is a wide band gap semiconductor whose potential device applications include UV lasers,[1,2] transparent conducting films for solar cells[3] and phosphors.[4] In addition to their excellent optical properties, high quality ZnO thin films are significantly easier to fabricate compared to GaN films, and they are attracting much attention as an alternative wide band gap semiconductor.[5] It is known that by mixing MgO (band gap 7.8 eV) with ZnO (3.3 eV), one can obtain a tunable band gap.[6,7]

Ability to detect and process signals at different wavelengths simultaneously is central in today's photonics technology. In order to detect signals at discrete wavelengths with high spectral resolution, present technology relies on arrays of waveguide gratings or thin-film filters. As the channel number continues to increase within a given bandwidth and the spectral separation between adjacent channel wavelengths gets smaller and smaller, integration of a large number of detection devices is expected to become precipitously more difficult and expensive. In the UV range, inexpensive wavelength distinguishable detectors are needed for a variety of medical, environmental, and military applications.[8–12] Here, we describe a simple and unique approach to fabricate monolithic broadband UV photodetectors with high tunable wavelength resolution using $Mg_xZn_{1-x}O$ composition-spread thin films.

The utility of composition spread/gradient samples has been previously demonstrated in rapid mapping of composition-property phase diagrams[13–16] as well as for optimizing materials properties.[17] In the present experiment, the entire spread acts as a single compact device for simultaneous detection of broadband signals.

In previous composition spread studies, the end compounds were typically isostructural, and thus structural changes of the material across the spread were limited to linearly changing lattice constants (following the Vegard's law).[13–15] Studies of solubility limits and phase separation of structurally disparate compounds are common themes in materials science, and they pose particularly interesting questions in thin film samples where nonequilibrium deposition processes and structural coherency with a compatible substrate can lead to formation of metastable phases. The present epitaxial composition spread has allowed us to completely map the phase evolution and separation processes in the $Mg_xZn_{1-x}O$ thin-film system. Precipitation of a cubic $Mg_xZn_{1-x}O$ phase [c-(Mg,Zn)O] segregated in the form of nanograins embedded in the host matrix of a hexagonal wurtzite $Mg_xZn_{1-x}O$ phase [h-(Zn,Mg)O] was observed, and an orientation relationship between c-(Mg,Zn)O and h-(Zn,Mg)O has been identified.

II. EXPERIMENT

For making the spreads, we have used our combinatorial pulsed laser deposition system which allows *in situ* epitaxial deposition of composition gradient samples. The details of

[a]Also at: Small Smart Systems Center, Department of Materials Science and Engineering, University of Maryland, College Park, Maryland 20742; electronic mail: takeuchi@squid.umd.edu
[b]Also at: Department of Materials Science and Engineering, University of Maryland, College Park, Maryland 20742.
[c]Also at: Center for Superconductivity Research, Department of Physics, University of Maryland, College Park, Maryland 20742.

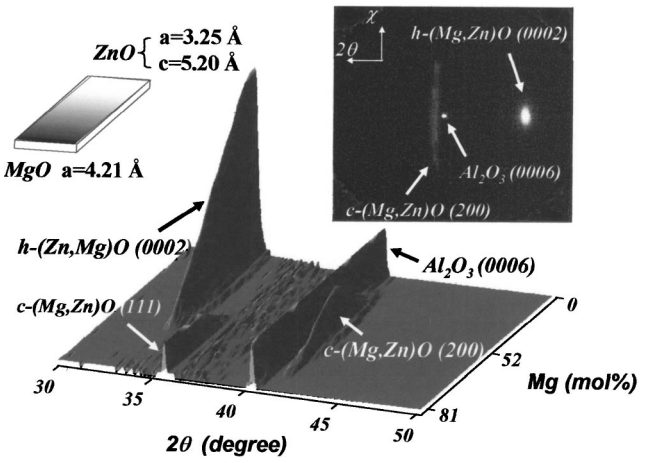

FIG. 1. X-ray diffraction of a $Mg_xZn_{1-x}O$ composition spread taken with a 300 μm diameter spot x-ray beam: 2θ vs composition with intensity integrated in χ in the range of $\pm 7.5°$ with respect to the substrate normal is shown. The composition range shown is from $x=0$ to 0.81. The total thickness at each position on a spread was typically 200 nm. The sample was approximately 6 mm long in the spread direction. The right inset is a χ–2θ diffraction intensity plot taken at $x=0.49$ on the spread. The left inset is a schematic of the spread chip and the lattice constants of the end compositions.

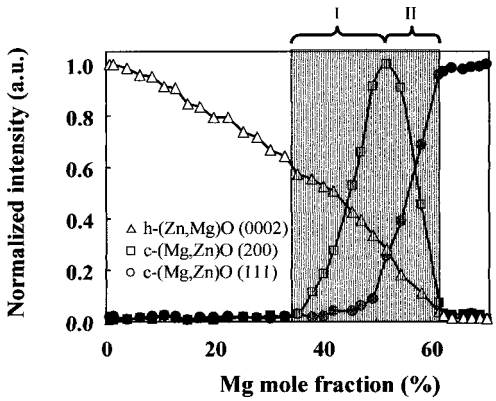

FIG. 2. The normalized x-ray intensity as a function of composition. The triangles, squares, and circles are from the *h*-(Zn,Mg)O (0002), *c*-(Mg,Zn)O (200), and *c*-(Mg,Zn)O (111) peaks, respectively. The linear change in the intensity of (0002) is primarily due to the continuous shift in the structure factor of the phase. The shaded area is the phase-separated region, and it is divided into regions I and II.

the system and the deposition process have been described elsewhere.[18,19] Two ceramic targets, ZnO and MgO, were ablated in an alternating manner for atomic layer-by-layer deposition onto (0001) sapphire substrates at 600 °C in 10^{-4} Torr of oxygen. The linear compositional variation across the spread was confirmed by wavelength dispersive spectroscopy. A scanning x-ray microdiffractometer (D8 DISCOVER with GADDS for combinatorial screening by Bruker-AXS) was used to characterize the out-of-plane lattice constants of the phases present in the film across the spread chip. High-resolution transmission electron microscopy (TEM) was performed at several positions on the spreads in order to investigate the microstructural properties of selected compositions. Optical transmission measurements was performed across the spread using an ultraviolet-visible (UV–VIS) spectrometer (200–800) nm with a aperture of 0.5 mm.

III. PHASE EVOLUTION AND STRUCTURE CHANGES ACROSS THE SPREAD

Figure 1 shows the 2θ versus composition plot from 30° to 50° and from ZnO to $Mg_{0.81}Zn_{0.19}O$. The diffraction was taken with the ω-scan mode, and at each 2θ, intensities are integrated in χ in the range of $\approx \pm 7.5°$. The relative change in the intensities of the peaks tracks the evolution of the phase changes as the composition is continuously varied. Starting from the pure ZnO end, the intensity of the (0002) peak from the wurtzite *h*-(Zn,Mg)O phase is seen to linearly decrease as x is increased. This is due to the continuous change in the structure factor of this phase as a function of composition. At around $x=0.45$, the peak from the (111) oriented *c*-(Mg,Zn)O starts to develop, and its intensity saturates at $x=0.6$ (Fig. 2). In addition, there is another peak at $2\theta \approx 42.6°$ which displays a transient behavior. Its 2θ value indicates that it is a (200) peak from the (100)-oriented *c*-(Mg,Zn)O. In previous studies, the presence of this orientation of the cubic phase had not been identified by x-ray or other characterization methods. This is most likely due to the fact that the orientation is not exact, and the phase is equally "distributed" in the χ range of $\pm 7.5°$ relative to the substrate normal. The right inset of Fig. 1 shows a χ–2θ intensity plot taken at $x=0.45$. It is evident that unless the diffraction data are integrated with respect to χ, the (200) peak may not be readily noticeable in an ordinary θ–2θ scan.

The phase-separated region is identified by the coexistence of x-ray peaks from the cubic and wurtzite phases. Compared to data from bulk $Mg_xZn_{1-x}O$,[20] we find that the solubility of Mg in the deposited ZnO-based wurtzite phase is significantly extended (from 2 to 37 mol %), while it is about the same for mixing Zn into the deposited MgO-based cubic phase (~40 mol %). These limits agree with previously reported values in thin-film $Mg_xZn_{1-x}O$.[6,21] In Fig. 2, we plot the normalized peak intensities versus composition. It is evident that in the phase separated region, *c*-(Mg,Zn)O is represented by both (100) and (111) orientations, and the (100)-oriented phase is associated with the presence of *h*-(Zn,Mg)O. Thus, just by studying the structural phase evolution in the spread, one can begin to gain insight into the physics of the phase separation process.

In order to further elucidate the transient nature and the microstructural origin of the phase separated region, cross-sectional TEM was performed. Figures 3(a) and 3(b) show a dark-field TEM image and a corresponding selected area electron diffraction (SAED) pattern, respectively, taken at approximately $x=0.5$ on a spread. Indexing of spots on the SAED pattern identifies reflections of the sapphire substrate (outlined with a dashed rectangle), *h*-(Zn,Mg)O (outlined with a solid line rectangle) and *c*-(Mg,Zn)O (encircled spots). From this we derive the following orientation relationship between the phases:

$$(0001)_{\text{sapphire}}//(0001)_{h\text{-(Zn,Mg)O}}//(100)_{c\text{-(Mg,Zn)O}};$$

$$(01\text{-}10)_{\text{sapphire}}//(2\text{-}1\text{-}10)_{h\text{-(Zn,Mg)O}}//(0-11)_{c\text{-(Mg,Zn)O}}.$$

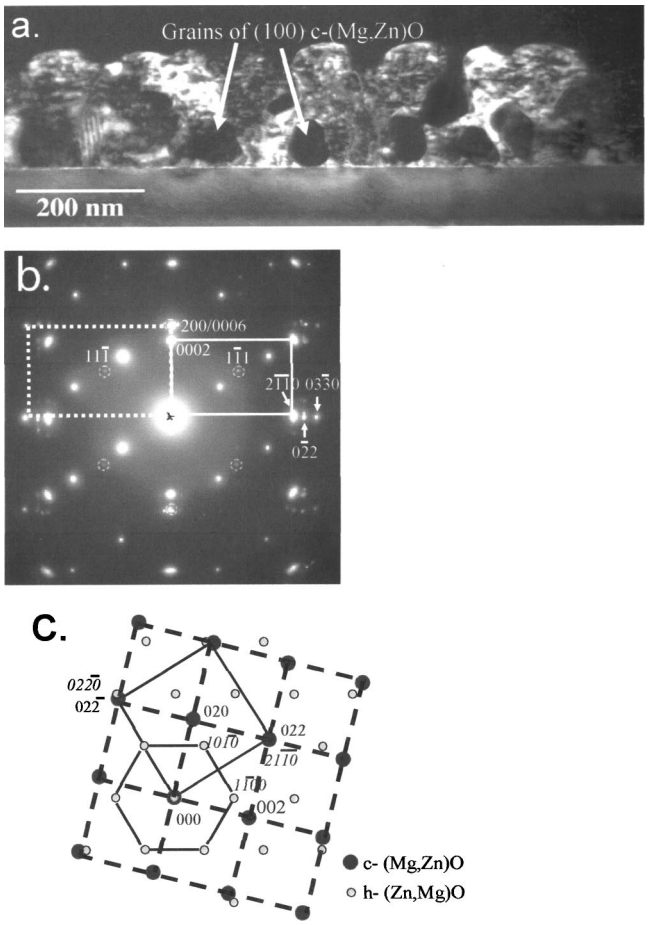

FIG. 3. (a) Cross-sectional TEM (dark-field) micrograph taken with the reflection of h-(Zn,Mg)O at $x=0.5$. (b) is a SAED of the same region. (c) The orientation relationship between the h-(Zn,Mg)O and (100) oriented c-(Mg,Zn)O viewed in reciprocal lattice space along [0001]/[100] direction.

The orientation relationship is an approximate one for c-(Mg,Zn)O considering the angular spread in positions of the (0−22) and (200) reflections, as seen in Fig. 3(b). The spread spans ±7.5° in deviation of the [100] of c-(Mg,Zn)O off [0001] of the substrate. This is consistent with the x-ray data in the spread in the distribution of spots in χ over ±7.5° with respect to the substrate normal as seen in the right inset of Fig. 1. The idealized orientation relationship is schematically illustrated in Fig. 3(c) in reciprocal space.

In Fig. 3(a) the dark regions belong to round-shaped nanograins of the (100)-oriented c-(Mg,Zn)O embedded into the matrix of h-(Zn,Mg)O. Electron dispersive spectroscopy of local regions indicates that the precipitated nanograins have a higher Mg concentration and the host has a higher Zn concentration compared to the composition given by $x=0.5$. The compositional difference between the coexisting phases and the roughness of a film surface suggest significant post/during deposition mass transport leading to the observed phase separation. In region I (Fig. 2), the initial deposition results in formation of a continuous film of a single phase of oversaturated h-(Zn,Mg)O. As the deposition progresses, the oversaturated h-(Zn,Mg)O precipitates the c-(Mg,Zn)O phase, which grows into the rounded grains. If the precipitation process were to produce (111) oriented c-(Mg,Zn)O, the

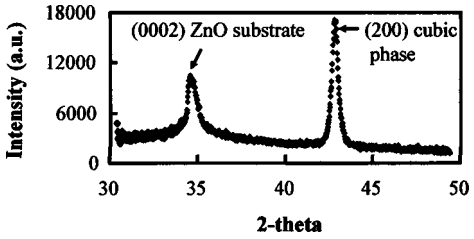

FIG. 4. 2θ diffraction plot of a 200-nm thick $Mg_{0.5}Zn_{0.5}O$ film deposited on a (0001) ZnO substrate. The intensity is integrated in χ in the range of ±7.5° with respect to the substrate normal.

match of c-(Mg,Zn)O and h-(Zn,Mg)O on the (111)/(0001) plane would result in a compressive plane stress. On the other hand, for the (100) orientation, there would be a good match between the (0,−1,1) planes of c-(Mg,Zn)O and (2,−1,−1,0)/(0,1,−1,0) of the h-(Zn,Mg)O matrix [Fig. 3(c)]. This results in a shear strain, which can be accommodated by a stress free precipitate/matrix interface during the nucleation stage. We speculate that the nucleation barrier is lower for (100) oriented c-(Mg,Zn)O than it is for (111) oriented c-(Mg,Zn)O. As one enters the region II in Fig. 2, there is a competing nucleation of (111) oriented c-(Mg,Zn)O growing directly on the substrate, and there is less and less h-(Zn,Mg)O, resulting in decreasing amount of (100) oriented c-(Mg,Zn)O nucleating out of oversaturated h-(Zn,Mg)O.[22]

The epitaxial relationship between the c-axis oriented hexagonal crystal and a (100) oriented cubic phase such as the one shown here has never been reported before. It can potentially be exploited to grow a wide variety of nonhexagonal materials epitaxially on c-axis oriented hexagonal substrates in a desirable orientation. By selecting orthorhombic (or tetragonal) materials with proper lattice matching, this orientational relationship can be made exact.[22] To check the occurrence of this growth relationship on a larger scale, we have grown a fixed composition $Mg_{0.5}Zn_{0.5}O$ film (200 nm thick) on a (0001) oriented ZnO substrate. The 2θ scan with χ integrated over ±7.5° of this sample (Fig. 4) displays only the (100) orientation consistent with the identified orientational relationship.

IV. OPTICAL PROPERTIES AND DEMONSTRATION OF MULTICHANNEL DETECTOR

Figure 5 shows the ultraviolet-visible transmission spectra from 200 to 400 nm measured across a spread in the region from $x=0$ to 0.65. Spectra display a clear continuous shift in the transmission edge. For the wurtzite $Mg_xZn_{1-x}O$, the transmittance reaches zero at about 380 nm for the pure ZnO, and at about 290 nm for the $Mg_{0.37}Zn_{0.63}O$. In this region, the transmission edge shifts a total of 90 nm at the rate of about 10 nm for every 4 mol % increase in Mg. The onset of phase separation is evident for compositions whose transmission edge starts at about 280 nm. In this region (shaded in the figure), the double edge transmission (marked by the arrows) arises from transmission through both the cubic phase and the wurtzite phase. Compared to its wurtzite counterpart, c-(Mg,Zn)O in the range close to MgO has a

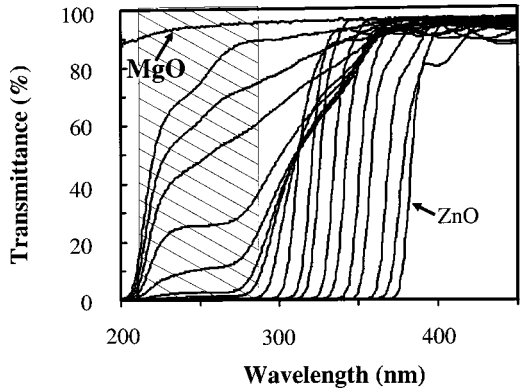

FIG. 5. UV–VIS photon transmission spectra of the composition spread $Mg_xZn_{1-x}O$ thin film for the Mg mole fraction from 0% to 64.8%. The shaded area is the phase separated region. The two arrows mark the approximate optical absorption edges due to the wurtzite and cubic phase of $Mg_xZn_{1-x}O$.

larger band gap, and this pushes the band gap dependent transmission edge to the shorter wavelength. The longest transmission edge wavelength from a single phase *c*-(Mg,Zn)O was found at around 230 nm. The band gap at different spots on the spread extracted from optical measurements are shown in Fig. 6. In the low Mg fraction region where the film remains wurtzite, the gap changes linearly from 3.27 to 4.28 eV. There is no well defined band gap between 4.3 and 5.4 eV, due to the phase separation. In the cubic single-phase end of the phase diagram, the band gap increases nonlinearly with increasing Mg fraction.

An array of Au interdigitated electrodes was deposited in order to fabricate metal–insulator–metal structures as photodetectors. Twenty-five detectors were fabricated along the length of one spread. Shown in Fig. 7 is the normalized spectral response of the photodetector array.[23] The position of the peak response wavelength shifts with the increase of Mg mole fraction from 380 nm for ZnO to 288 nm for wurtzite $Mg_{0.38}Zn_{0.62}O$. The detector with the peak wavelength at 206 nm is based on cubic $Mg_{0.69}Zn_{0.31}O$. The linewidth of the photon response spectra also varies with the film composition. As a figure of merit of a photodetector, we define the

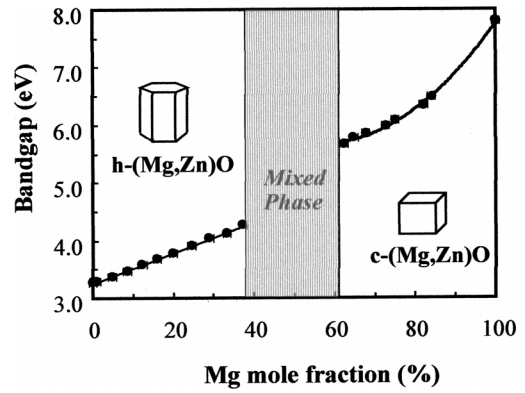

FIG. 6. Composition tuned $Mg_xZn_{1-x}O$ band gap and the corresponding phases. The shaded area is the phase separated region that has no well defined band gap. The band gap of pure MgO is represented by an open circle at $E_g = 7.8$ eV.

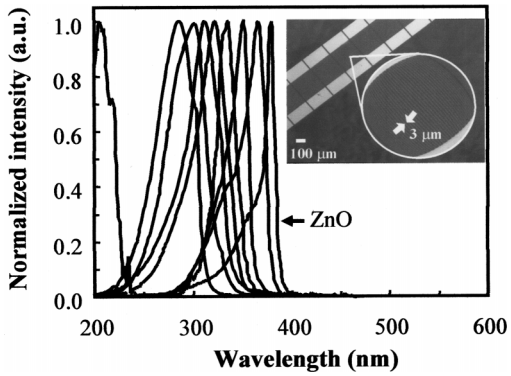

FIG. 7. Normalized spectral response of an array of UV photodetectors based on a composition spread of $Mg_xZn_{1-x}O$. The active area of each device was 250×220 μm^2. Composition variation within each detector is less than 2.4 mol %. The inset of Fig. 7 shows an enlarged picture of interdigited electrodes used as detectors. Each finger width and the finger separation is 3 μm. The electrodes were fabricated from a 200-nm-thick gold layer using the standard photolithography. Rapid thermal annealing at 400 °C for 1–2 min in the forming gas was applied to ensure good ohmic contact, which was verified by the linear $I-V$ curves.

useful "bandwidth" to be the difference between the peak response wavelength and the wavelength at which the response has dropped by 3 db on the longer wavelength side of the peak.[24] For the detector located at the pure ZnO end, this bandwidth is 4.5 nm. This number reaches the largest for a detector located at $Mg_{0.38}Zn_{0.62}O$ whose bandwidth is 17.3 nm. For *h*-(Zn,Mg)O with low Mg fractions, the line shape of the photon response is dominated by the exciton absorption. With increasing Mg, however, this exciton related feature seems to disappear gradually giving way to a broader background peak directly associated with the band gap. The broadening may be due to the change in the exciton population as a result of reduced exciton binding energy as a function of composition. A typical response time of an individual detector is 8 ns.

Despite the broadening, it is clear that, by adjusting the sizes of the spread and individual detectors and their arrangement, one can fabricate a composition-spread detector device with high and tunable wavelength resolution. This paves the way for intriguing device concepts including compact single-chip microspectrometers, where individual detector signals are multiplexed and digitally processed as different channels, and wavelength distinguishable UV dosimeters.

The use of entire composition-spreads as simultaneously active integrated devices opens up possibilities for a variety of other monolithic "functionally broadband" device components such as arrays of vertical cavity surface emitting lasers with a continuously changing emission wavelength and arrays of actuators with a continuously changing piezoelectric response.

V. CONCLUSION

We have made $Mg_xZn_{1-x}O$ composition spreads by the combinatorial pulsed laser deposition technique. The phase evolution across the spread was mapped using scanning x-ray microdiffractometry and transmission electron microscopy, and structural changes in different regions of the

spreads were investigated. An orientation relationship between (0001) oriented hexagonal (Zn,Mg)O and (100) oriented cubic (Mg,Zn)O was observed in the mixed region in the middle of the spread. This relationship can potentially be used to grow (100) oriented cubic structures heteroepitaxially on *c*-axis oriented hexagonal substrates. The concept of composition spread devices where a continuously varying functional parameter is used to assemble a type of device array is introduced. A broadband array of photodetectors based on the continuously changing band gap across the spread was demonstrated.

ACKNOWLEDGMENTS

This work was supported by Maryland Industrial Partnership and NSF DMR 094265 (CAREER), 0076456, and 0231291. The authors acknowledge useful discussions with J. M. Fitzgerald, R. P. Sharma, S. Choopun, S. Hullavarad, and O. O. Famodu.

[1] D. C. Reynolds, D. C. Look, and B. Jogai, Solid State Commun. **99**, 873 (1996).
[2] A. Ohtomo, K. Tamura, and M. Kawasaki, Appl. Phys. Lett. **77**, 2204 (2000).
[3] R. Groenen *et al.*, Appl. Surf. Sci. **173**, 40 (2001).
[4] T. G. Kryshtab *et al.*, Thin Solid Films **403**, 76 (2002).
[5] D. C. Look, Mater. Sci. Eng., B **80**, 383 (2001).
[6] A. Ohtomo, M. Kawasaki, T. Koida, K. Masubuchi, and H. Koinuma, Appl. Phys. Lett. **72**, 2466 (1998).
[7] Y. Matsumoto, M. Murakami, Z. Jin, and A. Ohtomo, Jpn. J. Appl. Phys., Part 2 **38**, L603 (1999).
[8] H. C. W. Eriksen, Photodermatol. **2**, 264 (1985).
[9] http://aura.gsfc.nasa.gov/instruments/omi/introduction.html.
[10] P. Schreiber, T. Dang, G. Smith, T. Pickenpaugh, P. Gehred, and C. Litton, Proc. SPIE **3629**, 230 (1999).
[11] S. Liang, H. Sheng, Y. Liu, Z. Huo, Y. Lu, and H. Shen, J. Cryst. Growth **225**, 110 (2001).
[12] W. Yang, R. D. Vispute, S. Choopun, R. P. Sharma, T. Venkatesan, and H. Shen, Appl. Phys. Lett. **78**, 2787 (2001).
[13] H. Chang, I. Takeuchi, and X.-D. Xiang, Appl. Phys. Lett. **74**, 1165 (1999).
[14] Y.-K. Yoo, F. Duewer, H. Yang, Y. Dong, J.-W. Li, and X.-D. Xiang, Nature (London) **406**, 704 (2000).
[15] T. Fukumura *et al.*, Appl. Phys. Lett. **77**, 3426 (2000).
[16] I. Takeuchi *et al.*, Nat. Mater. **2**, 180 (2003).
[17] R. B. van Dover, L. F. Schneemeyer, and R. M. Fleming, Nature (London) **392**, 162 (1998).
[18] K.-S. Chang, M. Aronova, O. O. Famodu, I. Takeuchi, S. E. Lofland, J. Hattrick-Simpers, and H. Chang, Appl. Phys. Lett. **79**, 4411 (2001).
[19] K.-S. Chang *et al.*, Mater. Res. Soc. Symp. Proc. **700**, 113 (2002).
[20] E. M. Levin, C. R. Robbins, H. F. McMurdie, and M. K. Reser (American Ceramic Society, Columbus, OH, 1964).
[21] A. K. Sharma, J. Narayan, J. F. Muth, C. W. Teng, C. Jin, A. Kvit, R. M. Kolbas, and O. W. Holland, Appl. Phys. Lett. **75**, 3327 (1999).
[22] The details of this analysis will be published elsewhere.
[23] The photocurrent of detector arrays was characterized using a low noise current preamplifier and a lock-in amplifier. A 150 W Xe lamp with 1200 line/mm grating monochrometer was used as the light source. The typical bias voltage for the detector is 5 V.
[24] For monolithic microspectrometer applications, sharp photon response edge to the right of the peak is more desirable since it allows higher wavelength resolution. Thus, we use the right half width at half maximum.